RSC Advances

ROYAL SOCIETY OF CHEMISTRY

www.rsc.org/advances

Journal Name

RSCPublishing

ARTICLE

High performance supercapacitor electrode material based on vertically aligned PANI grown on reduced Graphene oxide/$Ni(OH)_2$ hybrid composite

Cite this: DOI: 10.1039/x0xx00000x

Received 00th January 2012,
Accepted 00th January 2012

DOI: 10.1039/x0xx00000x

www.rsc.org/

Debasis Ghosh, Soumen Giri, Manas Mandal and Chapal Kumar Das*,

A simple and cost effective one pot hydrothermal process has been followed for the synthesis of flowery $Ni(OH)_2$, reduced graphene oxide (rGO)/$Ni(OH)_2$ hybrid composite. A ternary composite of rGO/$Ni(OH)_2$/PANI has also been synthesised by in situ oxidative polymerisation of anilne with the binary composite of rGO/$Ni(OH)_2$. A unique morphology of vertically aligned PANI on rGO surface and randomly connected PANI nanowire has been demonstrated following a hetarogeneous nucleation on the rGO surface and homogeneous nucleation inside the bulk material, respectively. A comparative electrochemical analysis reveals a superior electrochemical behavior of the ternary composite over the rGO-$Ni(OH)_2$, which again shows better electrochemical utility over the virgin $Ni(OH)_2$. The proton insertion/deinsertion reversible pseudocapacitance of $Ni(OH)_2$ combined with the pseudocapacitance of the vertically aligned conducting PANI nanowire and their synergistic effect with in situ reduced graphene oxide results in a high specific capacitance of 514 F/g at 2 A/g current density accompanied with 94.4% specific capacitance retention after 1000 charge discharge cycles at 5 A/g current density.

1. Introduction

Recent research on alternative energy resources is mainly centered on supercapacitor due to its high energy density at high power delivery rate accompanied with high cycle life performance. The charge storage mechanism of the supercapacitor electrode material involves either the electrical double layer (EDL) formation at the electrode/electrolyte interface or the faradaic reaction within the electrode material in presence of suitable electrolyte.[1] The total amount of charge stored in pseudocapacitor is many times higher than that of the EDLC materials, however, the later exhibits better cycle life than the pseudocapacitors.[1] carbonaceous materials such as activated carbon, carbon aerogel, carbon nanotube and graphene can act as active EDLC source due to their unique properties of high specific surface area and tunable porosity.[2] Amongst the carbonaceous materials graphene attracts the modern research most due to the unique properties of high surface area, high flexibility, high thermal and electrical conductivity and high capacitance.[3-6] Transition metal oxides/hydroxides such as, $Co(OH)_2$, $Ni(OH)_2$, MnO_2, SnO_2 are well known for their redox activity and effective pseudocapacitance in suitable electrolyte.[7-10] Amongst these pseudocapacitive materials $Ni(OH)_2$ is of most interest due to its easy processibility, various morphology, high redox activity, nontoxicity and overall lowcost.[11] Recent researches have established that a hybrid type material containing both pseudocapacitive and EDLC materials to be more effective in terms of both high capacitance and long cycle life.[12-14] Conducting polymers, such as polyaniline (PANI), polythiophene and polypyrrole are well known for their redox activity and can also act as pseudocapacitor. Amongst the various conducting polymers PANI is of most interest due to its unique properties of doping and dedoping in acid and base media, respectively, controllable electrical conductivity, easy and cost effective processability, etc.[15-16] Several investigation on PANI has revealed that it can act as efficient supercapacitor electrode material stand alone or with in a composite with CNT or graphene.[17-19]. But there are a few instance of a ternary composite of conducting polymers with metal oxide/ hydroxide and carbonaceous materials.[20-23]

Although the theoretical specific capacitance of $Ni(OH)_2$ is very high (2358 F/g with potential region of 0.44 V), the very low conductivity decreases the full utilization of electrode material and a close to optimum value can be obtained only in a very thin layer of material.[23] If the conductivity of the $Ni(OH)_2$ can be increased, the low charge transfer resistance can result in high specific capacitance. The conductivity of $Ni(OH)_2$ can be increased in a composite with conducting polymer (PANI) or highly conductive graphene. But with only PANI the problem of swelling and shrinking of the electrode material during charge discharge cannot be avoided. So if a ternary composite

of $Ni(OH)_2$/graphene/PANI is considered all the advantages of the three can come into act together for fabricating a superior electrode material, where, $Ni(OH)_2$ can acts as pseudocapacitor; graphene acts as EDLC source and increase the conductivity, surface area, porosity and flexibility of the composite, and PANI, apart from its pseudocapacitance can form a conductive interconnected network between $Ni(OH)_2$ and Graphene.

In our present study, we have synthesized a ternary composite of in situ reduced graphene oxide (rGO)/$Ni(OH)_2$/PANI by a two-step method. Firstly, reduced graphene/$Ni(OH)_2$ composite has been prepared by a one pot hydrothermal synthesis where graphene oxide is in situ reduced by urea and Ni^{2+}. In the second step in situ oxidative polymerization of aniline in presence of rGO/$Ni(OH)_2$ composite has been followed to prepare the ternary composite of rGO/Ni(OH)2/PANI.

2. Preparation of materials

2.1. Preparation of graphene oxide:

Graphene oxide was prepared following by a modified Hummer's method.[24] Briefly, in a mixture of 120 ml conc. H_2SO_4 and 13.3 ml H_3PO_4 1 gm graphite powder was added and sonicated for 10 minute. In the mixture, 6 gm $KMnO_4$ was added slowly in the suspension while stirring and the stirring was continued for 12 h maintaining the suspension temperature around 50°C. After that 1.5 ml 30% H_2O_2 in 135 ml ice water was slowly added to the mixture, cooled at room temperature and was stirred for another 4h and centrifuged at a low r.p.m. The brown precipitation was collected and repeatedly sonicated and centrifuged in acetone for four times and the final product was collected and dried at 60°C.

2.2. Preparation of reduced Graphene oxide/$Ni(OH)_2$ composite:

50 mg of the as prepared GO was well dispersed in a mixture of 20 ml 0.1 M $Ni(NO_3)_2$ and 20 ml 0.5 M urea by ultra sonicating using a ultrasonic horn for 1 h. Then the whole suspension was immediately transferred into a teflon sealed stainless steel autoclave of 50 ml capacity and maintained at 120°C for 8h and then allowed to cool at room temperature. The precipitation was collected and washed with ethanol water for several times and dried at 60°C. At high temperature in presence of Ni^{2+}, GO is reduced to graphene (reduced graphene oxide). The resulting black material was leveled as rGO/$Ni(OH)_2$.

2.3. Preparation of ternary composite:

The ternary composite was prepared using oxidative polymerization of aniline monomer in presence of rGO/$Ni(OH)_2$. Briefly, 0.3 ml aniline monomer was well dispersed in 100 ml ice water by ultrasonication for 5 minute. Then 190 mg of rGO/$Ni(OH)_2$ composite containing 50 mg rGO was added to it and again sonicated for two minute at a low power. 2 gm APS was dissolved in 100 ml ice water and the solution was poured drop by drop to the above suspension of rGO/$Ni(OH)_2$ containing aniline monomer while continuous stirring at 250 r.p.m. and the stirring was continued to 3h. The temperature of the bulk material was kept at 0-5°C during the whole stirring process. Then the whole material was kept in refrigerator overnight and then washed with water ethanol several times and the final precipitation was dried at 60°C. The prepared material was leveled as rGO/$Ni(OH)_2$/PANI.

3. Results and discussions

3.1 Materials characterizations

3.1.1. X-RAY DIFFRACTION ANALYSIS The XRD pattern of the as prepared rGO, $Ni(OH)_2$, rGO/$Ni(OH)_2$ and rGO/$Ni(OH)_2$/PANI are shown in Figure 1. For rGO film the strong peak at 2θ = 10.2° indicates the (001) plane. The XRD pattern of the as prepared $Ni(OH)_2$ exhibiting a very sharp peak centered on 2θ = 12.3° indicates the (003) plane. The medium frequency peaks at 2θ = 24.8°, 33.4° and 59.5° are indicative of the (006), (101) and (110) crystalline

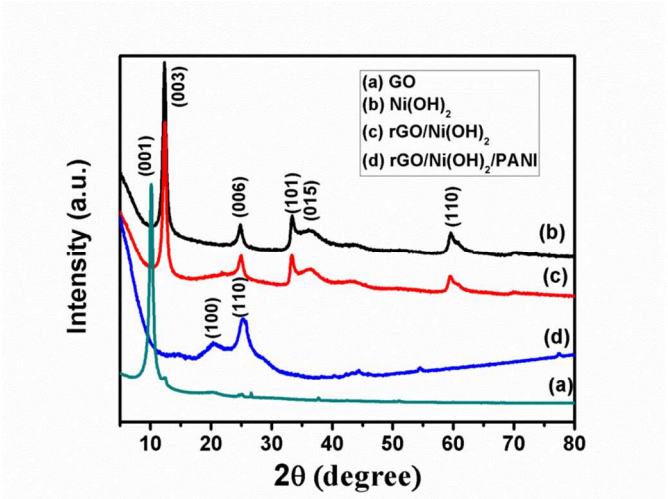

Figure 1. XRD analysis of the as synthesized GO, $Ni(OH)_2$, rGO/$Ni(OH)_2$ and rGO/$Ni(OH)_2$/PANI

plane, respectively. A broad peak can be observed within the range of 2θ = 34.5°- 38°, which belongs to the (101), (012) and (015) planes.[25] All these peaks confirms the α phase of the as prepared $Ni(OH)_2$.[25-27] In the XRD pattern of rGO-$Ni(OH)_2$ the crystalline peak of GO disappears and all the peaks of α $Ni(OH)_2$ re appears without any significant change confirming the reduction of the GO to graphene (rGO) by the Ni^{2+} and urea at 180°C. In the XRD pattern of the ternary composite, only characteristic peaks of PANI can be observed indicating successful coating of the amorphous PANI over the binary composite of rGO/$Ni(OH)_2$. The peak at 2θ = 20.4° and 25.2° indicates the periodicities parallel (100) and perpendicular (110) to the PANI chain respectively.[28] The presence of reduced graphene oxide in the composites was also confirmed by the Raman spectra and is shown in Figure S1 (see supporting information).

3.1.2 MORPHOLOGICAL ANALYSIS The morphological analysis of the as prepared materials was performed in terms of FESEM and TEM analysis and the images are shown in Figure 2 and Figure 3, respectively. 3D porous flower like architecture can be seen for the $Ni(OH)_2$. A close inspection of the flowery architecture reveals that the various interconnected sheet like petals with smooth surface

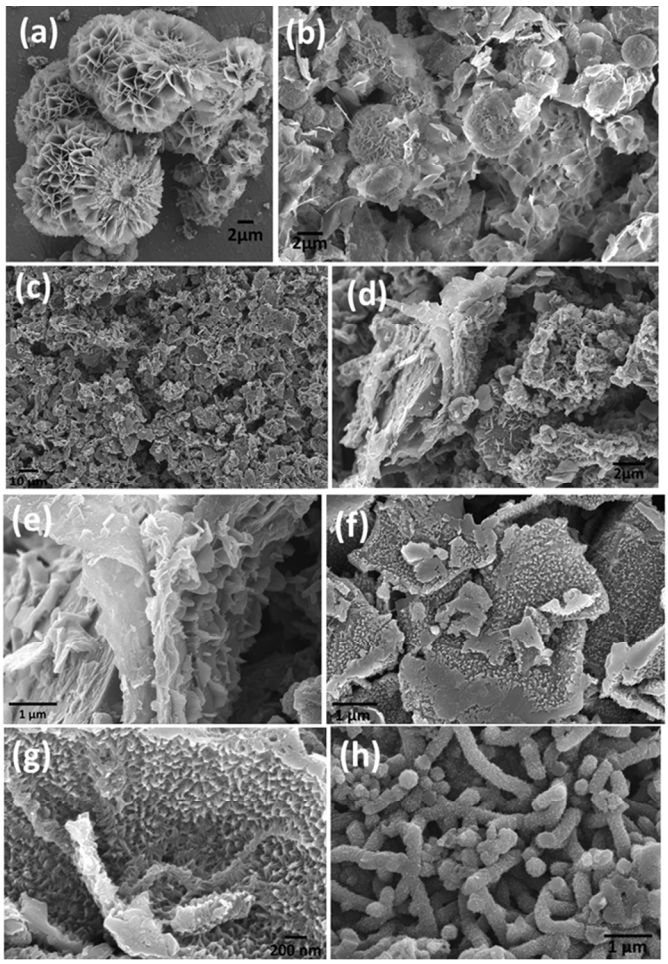

Figure 2. FESEM micrograph of (a) $Ni(OH)_2$ flower, (b) rGO wrapped $Ni(OH)_2$ flower, rGO/$Ni(OH)_2$/PANI composite (c) at low magnification, (d) at high magnification; (e, f, g) vertically aligned PANI over rGO surface in the rGO/$Ni(OH)_2$/PANI composite, (h) interconnected PANI nanowire

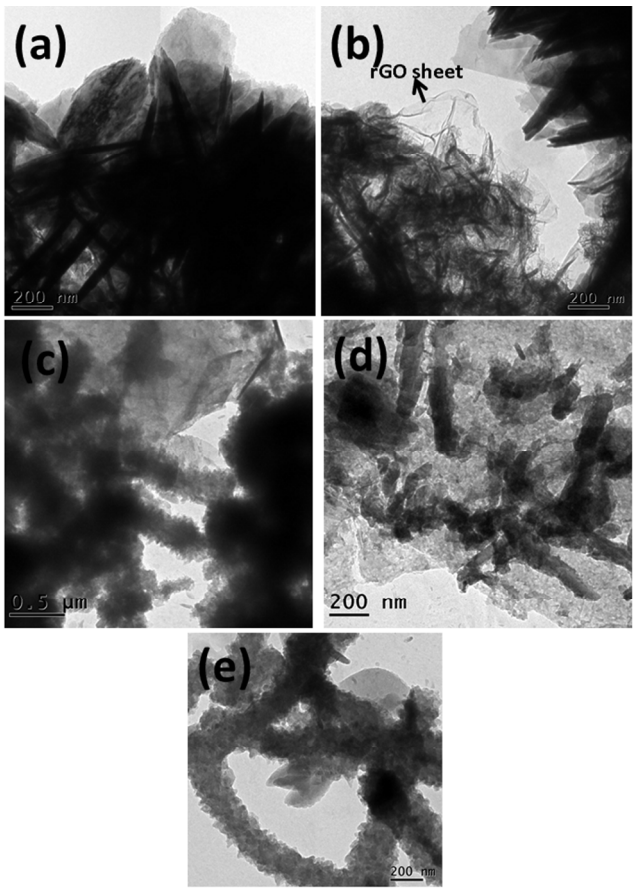

Figure 3. Tem image of (a) $Ni(OH)_2$ flower, (b) rGO/$Ni(OH)_2$ composite, (c) rGO/$Ni(OH)_2$/PANI composite, (d) vertically aligned PANI on rGO surface in rGO/$Ni(OH)_2$/PANI composite composite and (e) interconnected PANI nanowire network in rGO/$Ni(OH)_2$/PANI composite.

and thickness of ca. 50 nm are self-assembled to form the flowery architecture. Formation of the hierarchical flowery structure with smooth surface petal by a hydrothermal method involves dissolution and recrystallization process and with time being in order to minimize surface strain hierarchical flowery structure is obtained following a Ostwald ripening mechanism.[29-30] Surface morphology of the rGO-$Ni(OH)_2$ composite exhibits that the flowery architecture of the $Ni(OH)_2$ is well wrapped by the flexible rGO sheets (Figure 2b). Here rGO not only act as the basal plane for the growth of the flowery architecture, but also interconnects the various $Ni(OH)_2$ flowers. In case of the ternary composite (Figure 2c-2h) no individual $Ni(OH)_2$ was found possibly due to the excellent coating by the amorphous PANI. For the PANI, two types of morphology were found. Vertically aligned PANI grown on rGO sheet (Figure 2e, 2f, and 2g) and random connected PANI nanowires in the bulk material. At the starting of the polymerization most active nucleation sites generate on the solid rGO surface by a process of heterogeneous nucleation. Once the active site is generated it reduces the inter-facial energy barrier between the solid surface and bulk solution and renders the polymerization process where further PANI grows on the solid surface forming vertically aligned PANI over rGO surface.[31] Apart from the heterogeneous nucleation on solid surface, homogeneous nucleation occurs inside the bulk and randomly connected PANI nanowires are formed (Figure 2h), where aniline micelles act as the "soft template".[32-33]

The FESEM analysis was further supported by the TEM analysis as shown in Figure 3. As shown in Figure 3.a, the $Ni(OH)_2$ nano sheets are strongly interconnected to form $Ni(OH)_2$ flower. For the rGO/$Ni(OH)_2$ composites the $Ni(OH)_2$ nanopetals are well anchored on the rGO sheet as observed from Figure 3b. The little contrast between the rGO sheet and the carbon coated on copper grid indicates the ultrathin layer of the rGO in the binary composite. Vertically aligned PANI on rGO sheet in Figure 3d. and randomly connected PANI nanowire without any rGO substrate in Figure 3e. strongly supports the FESEM observation of the two types of PANI morphology in the ternary composite. However, for the rGO/$Ni(OH)_2$/PANI composite no individual $Ni(OH)_2$ flower was found from both the FESEM and TEM analysis indicating excellent coating of the PANI on the nanopetals forming the $Ni(OH)_2$ flowers.

The formation of $Ni(OH)_2$ flower and vertically aligned PANI on rGo/$Ni(OH)_2$ is shown in scheme 1.

Scheme 1 formation mechanism of $Ni(OH)_2$ flower and rGO/$Ni(OH)_2$/PANI composite

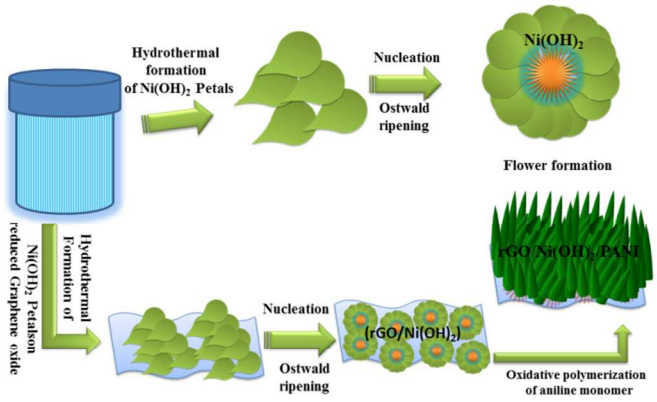

3.1.3 BET ANALYSIS In order to understand the effect of rGO and PANI on the surface area and pore size distribution of the binary and ternary composite with $Ni(OH)_2$ the BET analysis was carried out and is shown in Figure 4.

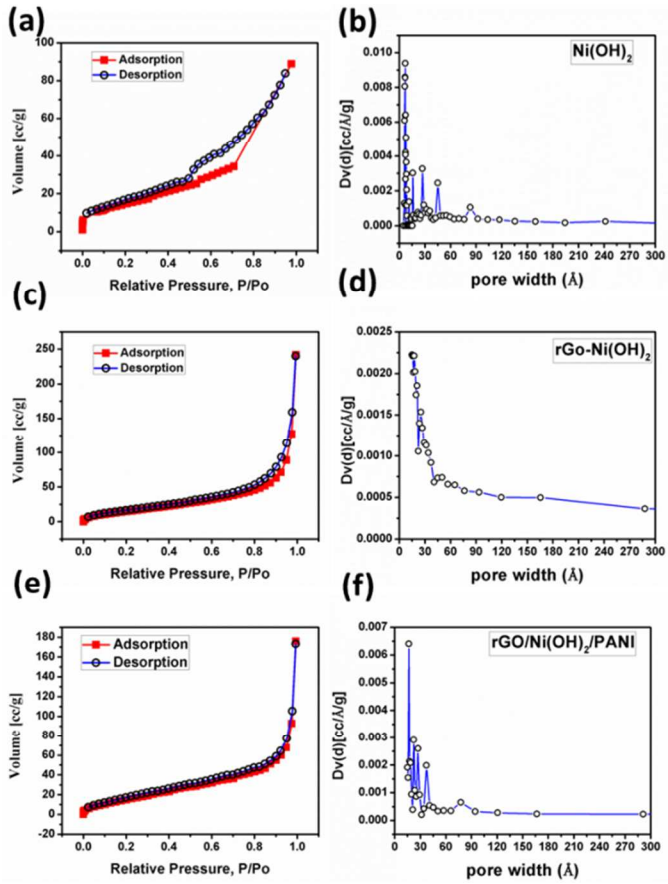

Figure 4. N_2 adsorption and desorption isotherm of (a) $Ni(OH)_2$, (c) rGO/$Ni(OH)_2$ and (e) rGO/$Ni(OH)_2$/PANI and their respective BJH pore size distribution (b), (d) and (f).

The inspection of the nitrogen adsorption and desorption isotherm of the $Ni(OH)_2$, rGO-$Ni(OH)_2$ and rGO/$Ni(OH)_2$/PANI at 77K is shown in Figure 4a, 4c and 4e, respectively manifesting a typical type IV isotherm with respective specific surface area of 54.56 m^2/gm, 62.729 m^2/gm and 66.371 m^2/gm. The type IV isotherm indicates the mesoporous nature of the as prepared materials. The increased surface area of the binary composite over virgin $Ni(OH)_2$ is due to the high surface area of graphene, which increase the overall surface area. The nano dimension of the PANI nanowire and vertically aligned PANI is responsible for the increased surface area of the ternary composite over the binary composite. The BJH pore size distribution of the $Ni(OH)_2$, rGO-$Ni(OH)_2$ and rGO/$Ni(OH)_2$/PANI is shown in Figure 4b, 4d and 4f, respectively. The pore size distribution exhibited a minor microporosity and a predominant mesoporosity within the range of 5-90 Å for $Ni(OH)_2$ and 15-90 Å for both the binary and ternary composites with respective maxima peak at 7.52 Å, 15 Å and 16.6 Å. An average pore diameter of $1.095e^{+02}$ Å, $2.39e^{+02}$ Å and 1.64 e^{+02} Å was calculated for the $Ni(OH)_2$, rGO-$Ni(OH)_2$ and rGO/$Ni(OH)_2$/PANI, respectively. An increased of average pore size of the binary composite is attributed to the presence of highly porous graphene, alternatively in the ternary composite surface coating by PANI results an decreased average pore size of the rGO/$Ni(OH)_2$/PANI composite.

3.2 Electrochemical characterizations

We first performed the GCD analysis of the as prepared electrode materials in order to evaluate the best working potential. The best working potential chosen for the $Ni(OH)_2$ and rGO-$Ni(OH)_2$ was from (-) 0.3 V to 0.4 V. For the Gr-$Ni(OH)_2$-PANI composite an increased working potential from (-) 0.3 V to 0.55 V was chosen. The working potential was chosen by considering the maximum coulombic efficiency. The GCD plots of the as prepared $Ni(OH)_2$, rGO/$Ni(OH)_2$ and rGO/$Ni(OH)_2$/PANI electrode are shown in Figure 5. at various constant charge discharge current densities of 2, 3, 4 and 5 A/g. The specific capacitances from the GCD plots was calculated using the equation

$$\text{Specific capacitance } c_{sp} = \frac{i*t}{m*\Delta v} \qquad (1)$$

where, i/m, t, and Δv represents the current density, discharge time and potential limit, respectively. The highest specific capacitance obtained from the $Ni(OH)_2$ electrode was 238 F/g at low current density of 2 A/g. For the rGO-$Ni(OH)_2$ electrode an increased specific capacitance of 359 F/g was obtained at 2 A/g current density. The improved specific capacitance generates from a combined EDLC effect of the rGO and pseudocapacitive effect of $Ni(OH)_2$ and their synergistic interaction. Low conductivity of $Ni(OH)_2$ causes a larger charge transfer resistance that restricts its specific capacitance to a lower value. Conductive graphene increases the overall electrical conductivity of the composite, which ensure high rate of charge transfer, hence high specific capacitance. For the ternary composite of rGO/$Ni(OH)_2$/PANI still increased specific capacitance of 514 F/g was achieved at 2 A/g current density. PANI itself is pseudocapacitive in nature, besides the vertically aligned PANI grown on rGO surface of the ternary composite and the nanowire PANI grown on $Ni(OH)_2$ results a better synergistic interaction amongst the three. PANI not only

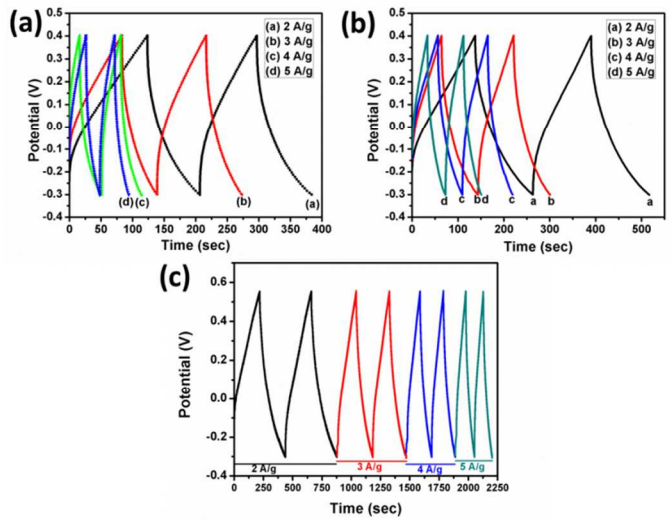

Figure 5. galvanostatic charge discharge plot of (a) $Ni(OH)_2$, (b) $rGO/Ni(OH)_2$ and (c) $rGO/Ni(OH)_2$/PANI at various constant current densities of 2, 3, 4 and 5 A/g.

increases the pseudocapacitance of the composite but also being a conductive polymer increases the overall electrical conductivity of the composite. Besides, the nano dimension increases the surface area of the composite. While performing the GCD test at higher current density of 5 A/g, high specific capacitance of 444 F/g was achieved for $rGO/Ni(OH)_2$/PANI ternary composite, which was far higher than that of virgin $Ni(OH)_2$ and $rGO/Ni(OH)_2$ electrode exhibiting specific capacitance of 156 F/g and 281 F/g, respectively. The ternary composite showed excellent rate capability in retaining specific capacitance of 86.3% at high current density of 5A/g with respect to the low current density of 2 A/g, which was better than the $Ni(OH)_2$ and $rGO/Ni(OH)_2$ composite with respective specific capacitance retention of 65.5% and 78.27%. The decreasing specific capacitance with increasing current density is due to the quick attainment of the voltage limit at high current in galvanostatic mode resulting in shortening of charging and discharging time. The variation of specific capacitance as a function of current density of all three electrodes is shown in Figure 9a. The coulombic efficiency from the charge discharge plot can be calculated from the equation

$$\text{Coulombic efficiency } (\eta) = (t_d/tc) \times 100\% \qquad (2)$$

where, t_d and t_c are the discharging and charging time, respectively. It is notable to mention that as the current density increases the coulombic efficiency increases for all the electrode material and for a particular current density of 2 A/g the coulombic efficiency was calculated as 96.2%, 98.1% and 97.6%, respectively for the $Ni(OH)_2$ and its binary and ternary composite, respectively. Higher the coulombic efficiency better is the reversibility of the electrode material. Presence of rGO increase the reversibility of the $rGO/Ni(OH)_2$ composite electrode, however another pseudocapacitive PANI in the ternary composite lowers the reversibility. The above observation demonstrates that it is only the rGO, which is responsible for the increased reversibility of the electrode material.

Energy storage material is known by its energy density and power density. Energy density from the GCD test can be calculated from the following equation

$$\text{Energy density } (E) = \tfrac{1}{2} C_s \times (\Delta V)^2 \qquad (3)$$

$$\text{Power density } (P) = E/T \qquad (4)$$

Where, C_s is the specific capacitance, ΔV is the potential limit and T is the discharge time of the charge discharge cycle from where the specific capacitance was calculated. At a power delivery rate of 700 W/kg the energy density of the $Ni(OH)_2$, $rGO/Ni(OH)_2$ was calculated to be 16.17, 24.45 Wh/kg, respectively. The larger working potential of the ternary composite resulted in a higher power density and the maximum energy density of 51.62 Wh/Kg was obtained at a power delivery rate of 850 W/kg. A significant energy density of 44.58 Wh/kg was obtained even at high power density of 2125 W/Kg indicating the excellent utility of the ternary composite as electrode material at high current. The various energy density and power density obtained for all the three electrodes are shown in a Ragone plot in Figure 6a.[34] In order to understand the cycle life of the electrode materials the charge discharge test was continued to 1000 consecutive cycles at 5 A/g current density and a specific capacitance retention of 86.5%, 94.7% was achieved respectively for $NI(OH)_2$ and $rGO/Ni(OH)_2$ at the end. The low cycle stability of $Ni(OH)_2$ can be attributed to its pseudocapacitive nature and the faradaic reaction results in swelling of electrode material. Flexible rGO sheets releases the strain involved with the consecutive charging and discharging

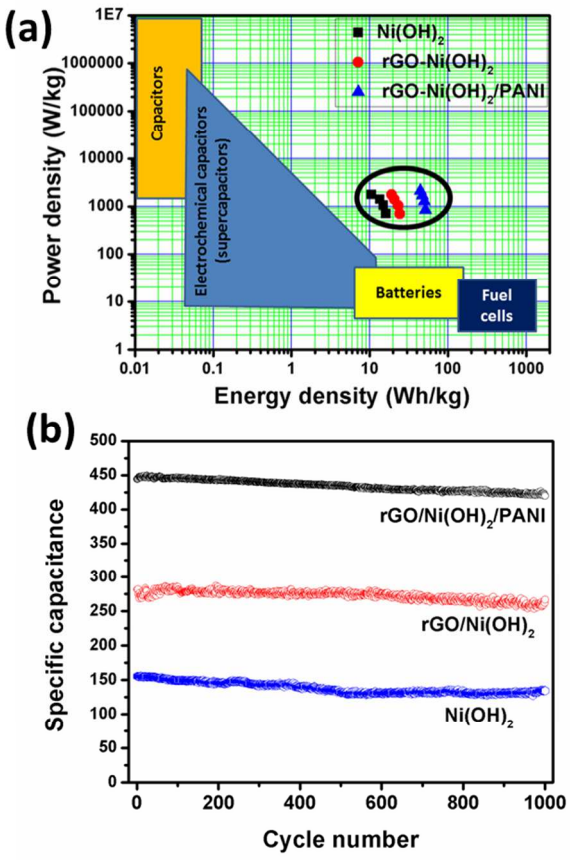

Figure 6. (a) Ragone plot of the $Ni(OH)_2$, $rGO/Ni(OH)_2$ and $rGO/Ni(OH)_2$/PANI electrode with a comparison of other energy storage systems, (b) variation of specific capacitance as a function of cycle number of the $Ni(OH)_2$, $rGO/Ni(OH)_2$ and $rGO/Ni(OH)_2$/PANI electrode.

of $Ni(OH)_2$, resulting in an increased cycle life of the binary composite. In case of the ternary composite it may be think that the cycle life would be low due to the possible deterioration of PANI after several dramatic shrinking and swelling charge discharge cycles. However stable electrochemical behavior of the ternary composite with 94.4% specific capacitance retention after 1000 cycles at 5A/g current density can be attributed to the vertically aligned PANI nanowire arrays on flexible rGO surface and their better synergistic effect. rGO sheets minimizes the mechanical deformation in the redox process of $Ni(OH)_2$ and PANI nanowire arrays and thus avoids electrode swelling and is beneficiary to high electrochemical stability of the ternary composite. Moreover, the vertical aligned PANI nanowire arrays were facile to strain reduction, which endorsed them to reduce the breaking during the process of counter ions doping/dedoping.[32]

Figure 7. demonstrates the CV plot of the porous $Ni(OH)_2$ electrode, $rGO/Ni(OH)_2$ and $rGO/Ni(OH)_2$/PANI electrode at various scan rates of 2, 10, 30 and 50 mV/s. All the plots deviate from perfect rectangular nature, which demonstrate the non-ideality of the electrode material and strongly support the predominant pseudocapacitor behavior. Unlike $Ni(OH)_2$ and $rGO/Ni(OH)_2$/PANI, the CV plots of $rGO/Ni(OH)_2$ shows some symmetrical behavior, possibly due to the rGO which act as EDLC source itself and its synergistic effect with pseucapacitive $Ni(OH)_2$ that results a close proximity towards ideal behavior of the $rGO/Ni(OH)_2$ electrode. The current response of all the electrodes increased with increasing the scan rate indicating that the electrode phenomenon is associates with a diffusion control process.

The specific capacitance from the CV plots was calculated from the equation below

$$\text{Specific Capacitance } C_{S=} \frac{\int_{V_1}^{V_2} i\,(V)\,dV}{(V_2 - V_1)\,\nu\,m} \qquad (5)$$

Where i is the instantaneous current response at any potential (V), V_2 and V_1 are upper and lower potential limit, ν and m are the scan rate and mass of the electroactive material, respectively. The various specific capacitance obtained at different scan rates are given in Table 1 and also presented in graphical form in Figure 9b. The highest specific capacitance obtained from the $Ni(OH)_2$ electrode was 269 F/g at 2 mV/s scan rate. The pseudocapacitance in $Ni(OH)_2$ in KOH electrolyte arises from the reversible redox reaction of proton insertion and de-insertion

$Ni(OH)_2 \leftrightarrow NiOOH + H^+ + e^-$

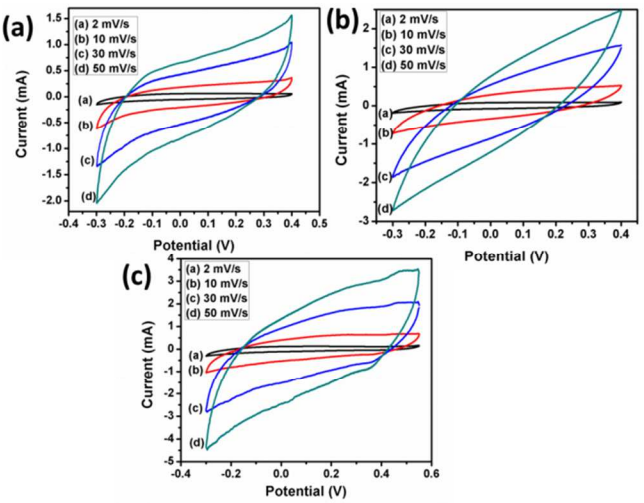

Figure 7. Cyclic voltammetry plots of (a) $Ni(OH)_2$, (b) $rGO/Ni(OH)_2$ and (c) $rGO/Ni(OH)_2$/PANI at different scan rates of 2, 10, 30 and 50 mV/s.

Table 1. Various specific capacitance obtained from the CV plot of the $Ni(OH)_2$, $rGO/Ni(OH)_2$ and $rGO/Ni(OH)_2$/PANI at different scan rates of 2, 10, 30 and 50 mV/s

Scan rate	2 mV/s	10 mV/s	30 mV/s	50 mV/s
$Ni(OH)_2$	`269 (F/g)	210(F/g)	177(F/g)	160(F/g)
rGO/ $Ni(OH)_2$	392(F/g)	331(F/g)	287(F/g)	261(F/g)
rGO/ $Ni(OH)_2$/PANI	539(F/g)	471(F/g)	412(F/g)	390(F/g)

The synergistic interaction of the porous $Ni(OH)_2$ with flexible rGO sheet results in improved specific capacitance of 392 F/g for the $rGO\text{-}Ni(OH)_2$ composite. The redox peaks of the $Ni(OH)_2$ is not prominent, this is a clear indication of the faradaic reaction to occur at a pseudo-constant rate over the entire volumetric cycle.[35] In case of the ternary composite the total specific capacitance increases as high as 539 F/g at 2 mV/s scan rate. The added PANI increases the total pseudocapacitance of the ternary composite that can be considered as the individual pseudocapacitance contribution from $Ni(OH)_2$, PANI and their synergistic interaction. PANI grown on the graphene surface are of nano dimension with excellent porosity and high surface area, which thereby increase the overall surface area of the $rGO/Ni(OH)_2$ composite. This ensures that plenty of ions can come in contact with the electrode material for a time and result high rate of charge transfer, hence high specific capacitance.

The electrodes were also analyzed by electrochemical impedance spectroscopy with in the frequency range of 1MHz to 10 mHz, and have been represented in terms of nyquist plot in Figure 8a after fitting with an equivalent electrical circuit (Figure 8b). All the nyquist plots exhibited similar nature of a depressed semicircle at initial high frequency followed by a straight line at an angle close to 45°. The high frequency semicircle indicates the presence of charge transfer resistance (Rct), the diameter of which determines the magnitude of Rct and the intercept with real impedance axis indicates the solution resistance (Rs). Although the electrolyte resistance are comparable for all three electrode materials, they notably differ in the R_{ct} with maximum of 93.8 ohm for $Ni(OH)_2$ and a gradual decreased Rct of 26.13 ohm and 13.89 ohm for the $rGO/Ni(OH)_2$ and $rGO/NI(OH)_2$/PANI, respectively. The decreased R_{ct} can be attributed to the presence of highly conducting rGO which increases the overall conductivity of the composite material. In case of the ternary composite conducting PANI forms several conducting tunnel within the composite

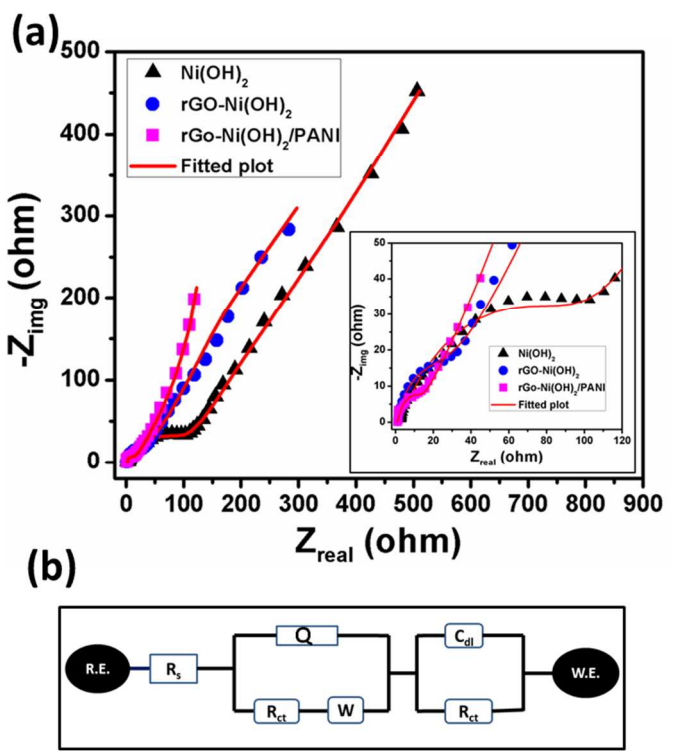

Figure 8. (a) Nyquist plot of $Ni(OH)_2$, $rGO/Ni(OH)_2$ and $rGO/Ni(OH)_2$/PANI and their magnified portion at high frequency (inset); (b) The equivalent electrical circuit to which the nyquist plots were fitted.

material through which the charge can effectively pass ensuring the lowest R_{ct}. The deviation of the post semicircle straight line from becoming parallel to the imaginary impedance axis indicates the non-ideality of the electrode materials and can be represented in terms of constant phase element (CPE). CPE (Q) exclude the real world capacitor and generates due to different defect in the electrode materials i.e. the edge defect, different coating thickness of electrode material on current collector, distribution of reaction sites, etc.[14] CPE constant (n) determines the ideality of the electrode material and a value closer to 1 indicates nearer ideal behavior. For the $Ni(OH)_2$, $rGO/Ni(OH)_2$ and $rGO/Ni(OH)_2$/PANI the CPE constant 'n' was found to be 0.76, 0.81 and 0.89, respectively. The post semicircle straight line inclined at an angle close to 45° indicates diffusion behavior of the electrode. A straight line with higher slope indicates lower diffusion resistance, hence high surface availability and higher ion accessibility. The presence of rGO is the main source of double layer capacitance of 1.1 F in the $rGO/Ni(OH)_2$ and 1.3 F in the $rGO/Ni(OH)_2$/PANI composite. The specific capacitance from the EIS was also calculated using the equation

$$\text{Specific capacitance} = (-)\, 1/(m \times 2\pi \times \mathrm{f} \times Z_{img})$$

Here, f, Z_{img}, and m, indicates the frequency, imaginary impedance and the electrode mass. The maximum specific capacitance obtained at low frequency of 0.01 Hz was 176 F/g, 281 F/g and 402 F/g, respectively for the $Ni(OH)_2$, $rGO/Ni(OH)_2$ and $rGO/Ni(OH)_2$/PANI composite electrode. The frequency dependent specific capacitance of the three electrodes is shown in Figure 9c. It is interesting to observe that the specific capacitance sharply decreases with increasing frequency, and the frequency response can be divided into three regions, a low frequency capacitor behavior, high frequency resistor behavior and a capacitor resistor combined behavior at lower middle frequency region.

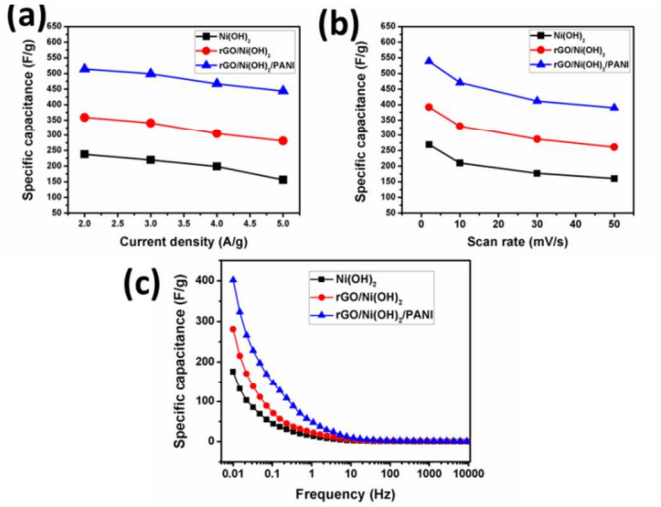

Figure 9. Variation of Specific capacitance as a function of (a) current density, (b) scan rate and (c) Frequency of $Ni(OH)_2$, $rGO/Ni(OH)_2$ and $rGO/Ni(OH)_2$/PANI

Conclusions

In this manuscript we have represented a cost effective hydrothermal procedure for the synthesis of $Ni(OH)_2$ and in situ reduced graphene oxide/$Ni(OH)_2$ composite, followed by an in situ oxidative polymerization of aniline with $rGO/Ni(OH)_2$ for the synthesis of $rGO/Ni(OH)_2$/PANI ternary composite. The porous flowery architecture and the effective pseudocapacitance of $Ni(OH)_2$ resulted in a specific capacitance of 238 F/g at 2 A/g. The excellent effectiveness of the pseudocapacitive $Ni(OH)_2$ was achieved in its composite with reduced graphene oxide with an increased specific capacitance of 359 F/g at 2 A/g current density accompanied with high cycle life. The unique morphology of the vertically aligned PANI on rGO surface and its high electrochemical activity resulted in a superior electrochemical behavior of the $rGO/Ni(OH)_2$/PANI ternary composite with 514 F/g specific capacitance at 2 A/g current density, which can be considered as the effective combined contribution of the pseudocapacitance of $Ni(OH)_2$ and PANI and their improved synergistic effect with the reduced graphene oxide. The high energy density of 51.62 wh/kg at a power density of 850 W/kg accompanied with long term cycle stability signify the $rGO/Ni(OH)_2$/PANI composite to be an superior supercapacitor electrode material.

Acknowledgements

The authors are thankful to UGC INDIA for funding and IIT Kharagpur for the instrumental help.

Notes and references

[a] Materials Science Centre, Indian Institute of Technology Kharagpur, Kharagpur-721302, India.

Electronic Supplementary Information (ESI) available: [Materials and instruments, electrode preparation, Raman spectra, GCD plots of rGO/Ni(OH)$_2$/PANI]. See DOI: 10.1039/b000000x/

1 B. Conway, Kluwer Academic/Plenum Publishers, New York, 2nd ed, 1999
2 J.-S. Lee, S.-I. Kim , J.-C. Yoon , J.-H. Jang, *ACS Nano*, 2013, **7,** 6047–6055
3 A .K. Geim, K.S. Novoselov, *Nat Mater.,* 2007, **6**, 183–191
4 H. Jiang, P. S. Lee, C. Li, *Energy Environ. Sci.* , 2013, **6**, 41-53.
5 S. Stankovich, D.A. Dikin, G.H.B. Dommett, K.M. Kohlhaas, E.J. Zimney, E.A. Stach, R. D. Piner, S. T. Nguyen, R. S. Ruoff, *Nature*, 2006, **442**, 282–286.
6 M.D. Stoller, S.J. Park, Y.W. Zhu, J.H. An, R.S. Ruoff, Nano Lett, 2008, **8**, 3498–3502
7 C. Yan, H. Jiang, T. Zhao, C. Li, J. Ma, P.S. Lee, *J. Mat. Chem.,* 2011**, 21**, 10482-10488.
8 H. B. Li, M. H. Yu, F. X. Wang, P. Liu, Y. Liang, J. Xiao, C. X. Wang, Y. X. Tong, G. W. Yang, *Nat. Comm.* 2013, **4**:1894, doi:10.1038/ncomms2932
9 A. Sumboja, C. Foo, X. Wang, P.S. Lee, *Adv Mat.*, 2013**, 25**, 2809-2815.
10 S.P. Lim, N.M. Huang, H.N. Lim, *Ceramics International*, 2013, **39**, 6647-6655.
11 J. Ji, L. L. Zhang, H. Ji, Y. Li , X. Zhao , X. Bai, X. Fan , F. Zhang, R. S. Ruoff, .*ACS Nano*, 2013, **7**, 6237–6243
12 D. Ghosh, S. Giri, C. K. Das, *ACS Sustainable Chem. Eng.,* 2013, ***1***, 1135–1142.
13 D. Ghosh, S. Giri, A. Mandal,C. K. Das, *Chem. Phys. Lett.,* 2013, **573**, 41-47.
14 D. Ghosh, S. Giri, C. K. Das *Nanoscale*, 2013,**5**, 10428-10437
15 Q. L. Hao , H. L. Wang, X. J. Yang, L. D. Lu, X. Wang , *Nano Res.*, 2011, **4**,323.
16 K. S. Ryu, Y. Lee, K.-S. Han, Y.J. Park, M. G. Kang, N.-G. Park, S. H. Chang, *Solid State Ionics,* 2004, **175**, 765–768.
17 A.Sumboja, X. Wang, J. Yan, P.S. Lee, *Electrochem. Acta*, 2012, **65**, 190-195.
18 D. Ghosh, S. Giri, A. Mandal, C. K. Das *Appl. Surf. Sci.,* 2013, **276**, 120–128.;
19 K. Zhang, L. L. Zhang, X. S. Zhao, J. Wu, *Chem. Mater.*, 2010, **22**, 1392–1401
20 X, Xia, Q, Hao, W, Lei, W, Wang, H, Wang, X. Wang, *J. Mater. Chem.,* 2012, **22**, 8314
21 X. Xia, Q. Hao, W. Lei, W. Wang, D. Sun, X. Wang, *J. Mater. Chem*., 2012, **22**, 16844–16850;
22 S. Giri, D. Ghosh, C. K. Das, (2013), *Adv. Funct. Mater.*.2014, **24**, 1312-1324
23 Y. Hou , Y. Cheng , T. Hobson J. Liu, *Nano Lett*., 2010, **10**, 2727–2733.
24 D. C. Marcano, D. V. Kosynkin, J. M. Berlin, A. Sinitskii, Sun, Z.; Slesarev, A.; L. B. Alemany, W. Lu,; J. M. Tour, *ACS Nano* 2010, **4**, 4806– 4814.
25 H. Wang, J. Gao, Z. Li, Y. Ge, K. Kan, K. Shi, *Cryst Eng Comm,* 2012, **14**, 6843–6852
26 M. H. Cao, X. Y. He, J. Chen, C. W. Hu, *Cryst. Growth Des.,*2007,**7**, 170–174.
27 P. Jeevanandam, Y. Koltypin, A. Gedanken, *Nano Lett.*, 2001,**1**, 263–266.
28 A. Sumboja , C. Y. Foo , J. Yan , C. Yan , R. K. Gupta, P. S. Lee, *J. Mater. Chem.* , 2012, **22**, 23921-23928.
29 H. Du , L. Jiao, K. Cao , Y. Wang, H. Yuan, *ACS Appl. Mater. Interfaces*, 2013, **5**, 6643–6648
30 X.W. Lou, C. Yuan, E. Rhoades, Q. Zhang, L.A. Archer, *Adv. Funct. Mater.*, 2006, **16**, 1679.
31 N.-R. Chiou, C. M.Lui, J. J. Guan, L. J. Lee, A. J. Epstein, *Nat. Nanotechnol*.2007, **2**, 354–357.
32 J. Xu, K. Wang, S.-Z. Zu, B.-H. Han, Z. Wei, *ACS Nano*, 2010, **4**, 5019–5026.
33 Z. M. Zhang, Z. X. Wei, M. X. Wan, *Macromolecules*, 2002, **35**, 5937–5942.
34 M. S. Halper, J. C. Ellenbogen, Supercapacitor: A Brief Overview, Mar. 2006. [Online]. Available: http://www.mitre.org
35 X. Lang, A. Hirata, T. Fujita, M. Chen, *Nat. Nanotechnol.*, 2011, **6**, 232–236.

Table of content

Unique vertically aligned PANI on rGO/$Ni(OH)_2$ composite has been synthesized by a hydrothermal method exhibiting superior electrochemical behavior.